Title

Conformations of peptoids in nanosheets result from the interplay of backbone energetics and intermolecular interactions

Permalink

https://escholarship.org/uc/item/15q52427

Journal

Proceedings of the National Academy of Sciences of the United States of America, 115(22)

ISSN

0027-8424

Authors

Edison, John R
Spencer, Ryan K
Butterfoss, Glenn L
et al.

Publication Date

2018-05-29

DOI

10.1073/pnas.1800397115

Peer reviewed

Conformations of peptoids in nanosheets result from the interplay of backbone energetics and intermolecular interactions

John R. Edison[a], Ryan K. Spencer[a,b], Glenn L. Butterfoss[c], Benjamin C. Hudson[d], Allon I. Hochbaum[b], Anant K. Paravastu[d], Ronald N. Zuckermann[a], and Stephen Whitelam[a,1]

[a]Molecular Foundry, Lawrence Berkeley National Laboratory, Berkeley, CA 94720; [b]Department of Chemical Engineering & Materials Science, University of California, Irvine, Irvine, CA 92697; [c]Center for Genomics and Systems Biology, New York University Abu Dhabi, Abu Dhabi, United Arab Emirates; and [d]School of Chemical & Biomolecular Engineering, Georgia Institute of Technology, Atlanta, GA 30332

The conformations adopted by the molecular constituents of a supramolecular assembly influence its large-scale order. At the same time, the interactions made in assemblies by molecules can influence their conformations. Here we study this interplay in extended flat nanosheets made from nonnatural sequence-specific peptoid polymers. Nanosheets exist because individual polymers can be linear and untwisted, by virtue of polymer backbone elements adopting alternating rotational states whose twists oppose and cancel. Using molecular dynamics and quantum mechanical simulations, together with experimental data, we explore the design space of flat nanostructures built from peptoids. We show that several sets of peptoid backbone conformations are consistent with their being linear, but the specific combination observed in experiment is determined by a combination of backbone energetics and the interactions made within the nanosheet. Our results provide a molecular model of the peptoid nanosheet consistent with all available experimental data and show that its structure results from a combination of intra- and intermolecular interactions.

peptoid secondary structure | biomimetic sequence-specific polymers | cis-amide | 2D supramolecular assembly

T he shape of a molecule influences how it packs and assembles, and the interactions made upon assembly can influence the shape of the molecule (1). This interplay is seen in simple molecules with few degrees of freedom (2) and in complex molecules, such as proteins, with many degrees of freedom (3). Thus, the conformations of molecules in self-assembled structures do not reflect the ensemble of conformations accessible in solution, and inspection of the conformations of a single molecule does not necessarily suggest which one it adopts, or what super-structure it makes, upon self-assembly. Here we use classical and quantum simulation methods and experimental data (4) to extend our understanding of the local conformations and molecular order of peptoid polymers within bilayer nanoscale assemblies called nanosheets. The residues of nanosheet-forming peptoids are arranged in an alternating sequence of hydrophobic and hydrophilic monomers, with the latter having opposite charge and being segregated by charge type. A variety of peptoid sequences that obey this general design principle self-assemble into extended flat nanostructures (5–8). Our previous simulations (9) predict that nanosheets are flat because their constituent polymers are linear and untwisted, by virtue of adjacent backbone elements adopting twist-opposed rotational states. Atomic distances probed with PITHIRDS-constant time dipolar recoupling solid-state NMR (4) are consistent with this general principle, but not with the specific rotational states seen in the previous model. Here we use these data to produce a refined model of the nanosheet that is consistent with all current experimental data. Peptoid back-bones within this refined model also display alternating rotational states, allowing them to remain linear and untwisted, but the states

are such that the packing and interactions within the nanosheet are optimized at the expense of incurring some backbone strain. That is, the molecular conformations consistent with experiment are not obvious from inspection of the properties of individual strands, but are selected by the interactions between peptoids in nanosheets.

In what follows we describe our study. We begin by assessing the configuration space within which peptoid polymers can be made linear, a prerequisite for their formation into flat, extended structures. We show that different molecular structures are consistent with extended nanosheets and that the combination consistent with experiment results in a densely packed structure displaying a high degree of order.

Designing Linear Peptoid Polymers

The local or secondary structure of peptoids is defined by the rotational state of the backbone and specified by the dihedral angles ϕ, ψ, and ω (Fig. 1 A and B). As in peptides, the latter usually fluctuates around one of two values, defining *trans* ($\omega \approx 180$) and *cis* ($\omega \approx 0$) conformations (10, 11), while ϕ and ψ vary in a more continuous fashion and span what is known as the Ramachandran diagram (12, 13). Experiments (5–7) and simulations of nanosheets (7, 9) suggest that successive peptoid residues display their side chains in opposing directions, so that aromatic residues form the interior of the nanosheet and charged residues are exposed to water. Thus, the rotational state of a nanosheet-forming peptoid is defined by the rotational states of two successive residues, $\{\phi_i, \psi_i, \omega_i\}$ and $\{\phi_{i+1}, \psi_{i+1}, \omega_{i+1}\}$. Molecular dynamics simulations of nanosheets (9) indicate that

Significance

Commonly observed secondary structures of proteins, such as α-helices and β-sheets, are built from a *trans*-amide backbone with residues sampling a single region of the Ramachandran plot. Here we report a secondary structure displayed by biomimetic peptoid polymers in which the backbone exhibits the *cis* conformation and alternating residues display rotational states of opposed (pseudo)chirality. This structure is linear and untwisted and enables strands to pack densely into extended bilayer nanosheets.
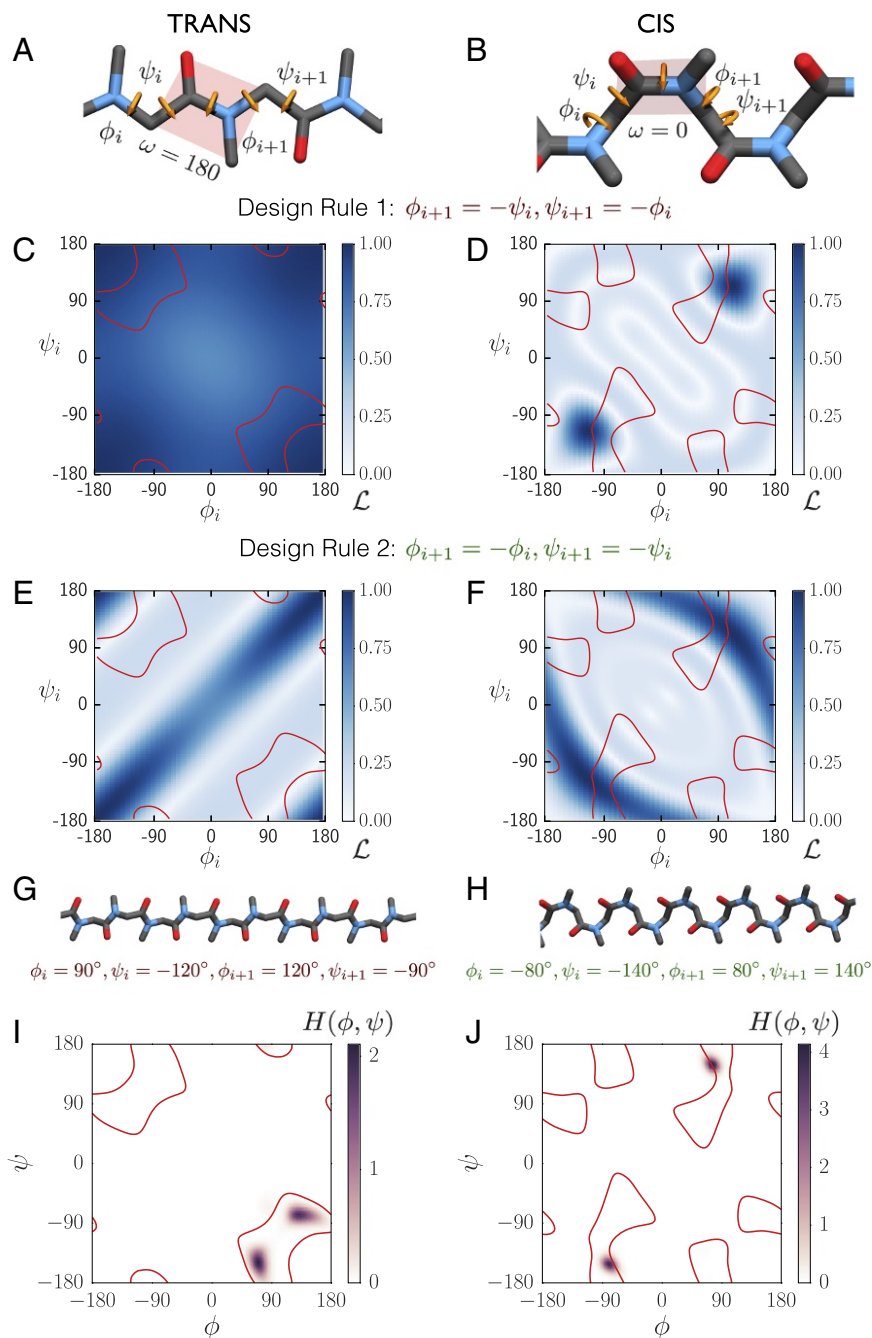
Fig. 1. The *trans*-peptoid backbone is disposed toward linearity, but the form observed in nanosheets is *cis*. (*A* and *B*) Schematic of a *trans*- (*A*) and *cis*- (*B*) peptoid backbone showing the dihedral angles of two adjacent residues, *i* and *i* + 1. (*C* and *D*) Linearity (actual length divided by maximum possible length) $\mathcal{L}$ of an eight-residue *trans*-polysarcosine (*C*) and *cis*-polysarcosine (*D*) as a function of backbone dihedral angles ϕ_i and ψ_i. Here the dihedral angles of successive residues satisfy $(\phi_{i+1}, \psi_{i+1}) = (-\psi_i, -\phi_i)$ (opposed twist). The red contours shown indicate regions that lie within 4 kcal/mol of the minima in the free-energy landscape of a disarcosine peptoid in vacuum. *E* and *F* are the same as *C* and *D*, but under the design rule $(\phi_{i+1}, \psi_{i+1}) = (-\phi_i, -\psi_i)$ (opposed chirality). *G* and *H* show candidate structures used to build models of nanosheets for MD simulations, using design rules 1 and 2, respectively. *I* and *J* are Ramachandran probability plots obtained from MD simulations of all-*trans* and all-*cis* polymers in nanosheets.

successive residues spontaneously adopt an alternating pattern in which (on average) $(\phi_i, \psi_i) = (75°, -145°)$ and $(\psi_{i+1}, \phi_{i+1}) = (135°, -75°)$. These values are related by a reflection about the negative-sloping diagonal of the Ramachandran plot (12, 13); i.e., they are twist-opposed states that satisfy $(\phi_{i+1}, \psi_{i+1}) = (-\psi_i, -\phi_i)$. Those simulations were initiated with residues in the *trans* state ($\omega_i = \omega_{i+1} \approx 180$), a conformation that disposes the peptoid backbone toward linearity. For *trans* residues, any choice of angle pairs of this nature causes the bonds N-C$_\alpha$ of residue *i* and C$_\alpha$-C$_O$ of residue *i* + 1 to point in the same direction (Fig. 1*A*) and so produces linear, untwisted strands (Fig. 1*C*). The same is not true of *cis* residues (Fig. 1*B*), for which only a small subset of the Ramachandran diagram leads to linear strands (Fig. 1*D*). Moreover, the regions of the Ramachandran plot favored energetically by the isolated peptoid backbone (enclosed by the red contours in Fig. 1 *C* and *D*) are consistent with linear strands for the *trans* backbone but not for *cis*. A similar conclusion is drawn by considering, in Fig. 1*F*, the linearity of *cis* strands under a second design rule, in which adjacent rotational states possess opposing chirality. Such states satisfy

$(\phi_{i+1}, \psi_{i+1}) = (-\phi_i, -\psi_i)$ and are related by successive reflections in the two diagonals of the Ramachandran plot. This design rule was studied earlier in the context of polypeptides with alternating D and L amino acids (10, 14). A small section of the energetically favored region of the Ramachandran plot corresponds to linear strands, but much less than *trans* under the previous rule (Fig. 1*C*).

Thus, a geometrical analysis of the peptoid backbone indicates that the *trans* conformation achieves linearity of the backbone in a way that is natural in a geometric sense and preferred in an energetic sense. However, new solid-state NMR experiments indicate that peptoid backbones in nanosheets are predominantly *cis* (4). The NMR study focused on backbone residues 7, 8, and 15, because our simulations predict that these residues experience different environments (Fig. 2). The residues of nanosheet-forming peptides are alternately hydrophobic and hydrophilic, with the latter having opposite charge and being segregated into blocks by charge type (Fig. 2 *A* and *B*). As a
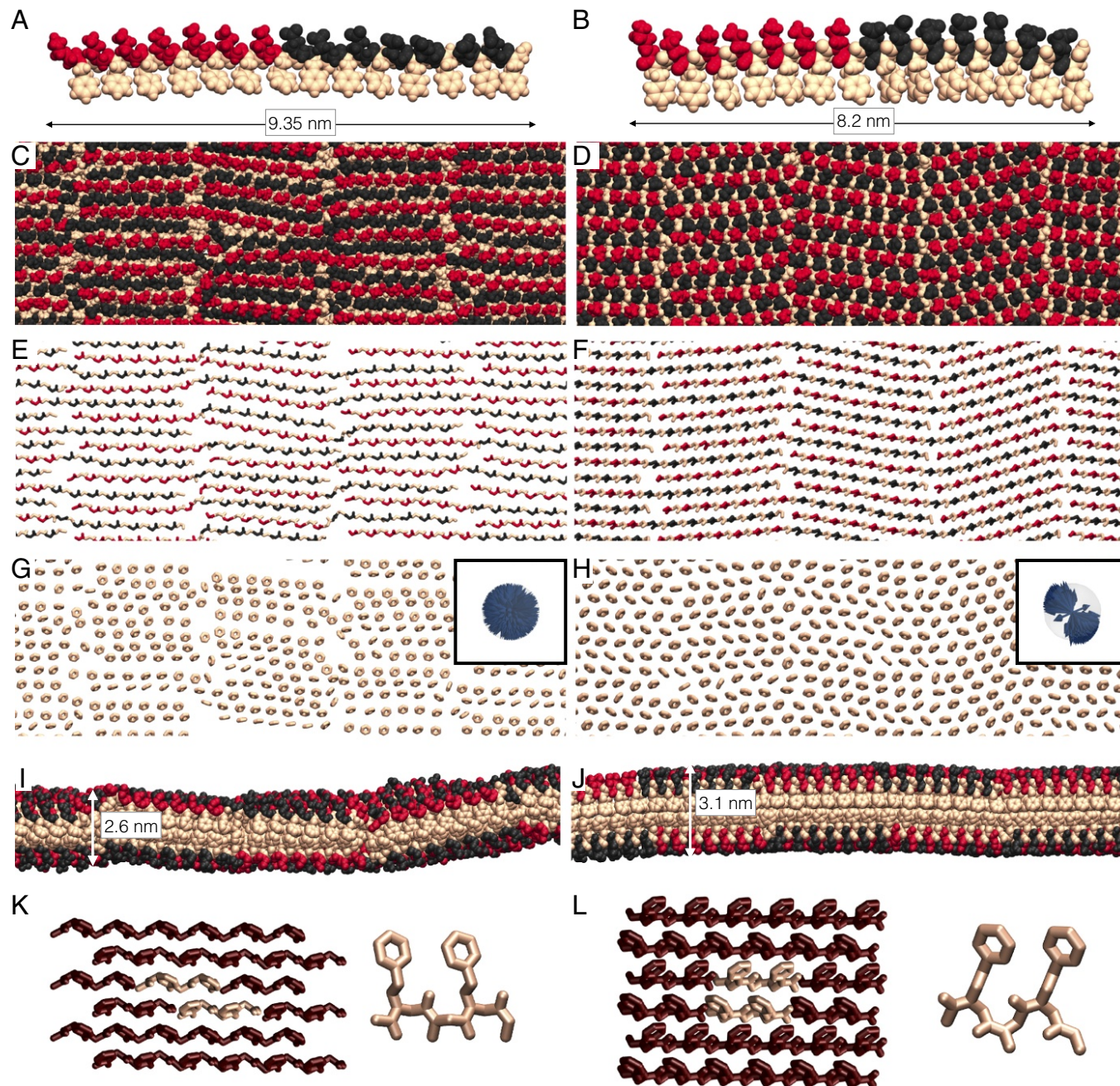
Fig. 2. The *cis* nanosheet (*B*, *D*, *F*, *H*, *J*, and *L*) is more ordered and more densely packed than the *trans* nanosheet (*A*, *C*, *E*, *G*, *I*, and *K*). (*A* and *B*) A single peptoid taken from a nanosheet, with atoms colored by residue name. In *A–J* positively charged *N*-(2-aminoethyl) glycine residues are shown in red, negatively charged *N*-(2-carboxyethyl) glycine residues are shown in black, and *N*-(2-phenylethyl) glycine residues are shown in tan. (*C* and *D*) Top views of nanosheets. (*E* and *F*) Top view of the backbone atoms of the top layer of nanosheets. (*G* and *H*) Phenyl rings belonging to the top layer of nanosheets. *Insets* show the orientation distribution of the phenyl groups plotted on a unit sphere. (*I* and *J*) Side views of the nanosheets. All renderings are done from MD configurations using visual molecular dynamics (VMD) (15) and Persistence of Vision Raytracer. (*K* and *L*) Top view of alternating sarcosine, *N*-(2-phenylethyl) glycine monolayers optimized using ab initio simulations at the M06-2X/6-31G* level of theory under 2D periodic boundary conditions (unit cell shown in tan and replicates in maroon). We also show the side view of one of the strands to highlight the backbone structure (compare with Fig. 1 *G* and *H*).

result, the electrostatic energy of the nanosheet is minimized when polymers adopt a "brick" configuration in which certain residues, including residues 7 and 8, sit adjacent to residues in neighboring peptoids, while residue 15 sits adjacent to gaps in the structure (7, 9). NMR shows that residues 7 and 8 in peptoid backbones adopt the *cis* conformation with high probability and that residue 15 is equally likely to be *cis* or *trans*, thereby indicating that these residues indeed experience different environments in the nanosheets. The high *cis* propensity of residues 7 and 8, however, is not consistent with the existing nanosheet model (9) and therefore warrants another modeling study.

Nanosheet Design

To perform this study we built two versions of the nanosheet, using either all-*trans* or all-*cis* backbones; details can be found in *SI Appendix, 1. Simulation setup*. We used a staged scheme to obtain ordered nanosheets. First, we built peptoid polymers into brick nanosheet structures (7, 9), solvated them, and simulated them using Nanoscale Molecular Dynamics (NAMD) (16) in the NPT (fixed number of particles N, pressure P, temperature T) ensemble (simulations done using the constant-tension ensemble yielded similar results). Upon initial relaxation some parts of these nanosheets became disordered, but a majority of backbones adopted the ordered forms shown in Fig. 1 *G* and *H*. These are Σ ("sigma") strands (9) whose residues alternate between the rotational states shown in Fig. 1 *I* and *J*, respectively [the *cis*-Σ strand's rotational states are similar to those of the "ω-strand" motif found in crystalline peptoid trimers (17)]. Second, we built structures in which all polymers were initialized with these rotational states (*SI Appendix*, Fig. S1); these nanosheets remained stable and ordered upon 200 ns of simulation.

In Fig. 2 we show that the *cis* nanosheet is more densely packed ($\simeq$31% more chains per unit area) and has a higher degree

of order than the *trans* nanosheet. The backbones of the *cis* nanosheet are linear, with the exception of a kink at the middle residue (which sits adjacent to gaps in the brick pattern), and the phenyl rings in the interior of the sheet exhibit both positional and orientational order. As a result, the interpeptoid interactions made in the *cis* nanosheet are more favorable than those made in the *trans* nanosheet, and the sum of the intra- and interpeptoid energies per molecule of the *cis* nanosheet is lower, by about 9 $k_B T$ (5.3 kcal/mol) per residue, than that of the *trans* nanosheet. In other words, the interactions made by peptoids within the *cis* nanosheet compensate for the penalty incurred to keep the *cis* backbone in a linear configuration.

Our quantum mechanical calculations are consistent with structures obtained from molecular-dynamics simulations. Model chains of alternating sarcosine, *N*-(2-phenylethyl) glycine residues optimized at the M06-2X/6-31G* level of theory (18) under 2D periodic boundary conditions with a unit cell of two four-residue chains yield all-*trans* and all-*cis* strands consistent with the Σ motifs shown in Fig. 2 *K* and *L* (compare with Fig. 1 *G* and *H*). The aromatic rings in the phenyl layer of the all-*cis* system

Table 1. Experimental and simulation measurements

Measurement	Value, Å	Experimental technique	Simulation *trans*, Å	Simulation *cis*, Å
Thickness of nanosheets	30	AFM	26	31
Spacing between strands	4.5	XRD	4.8	4.45
Lamellar spacing between sheets	28	XRD	23	30

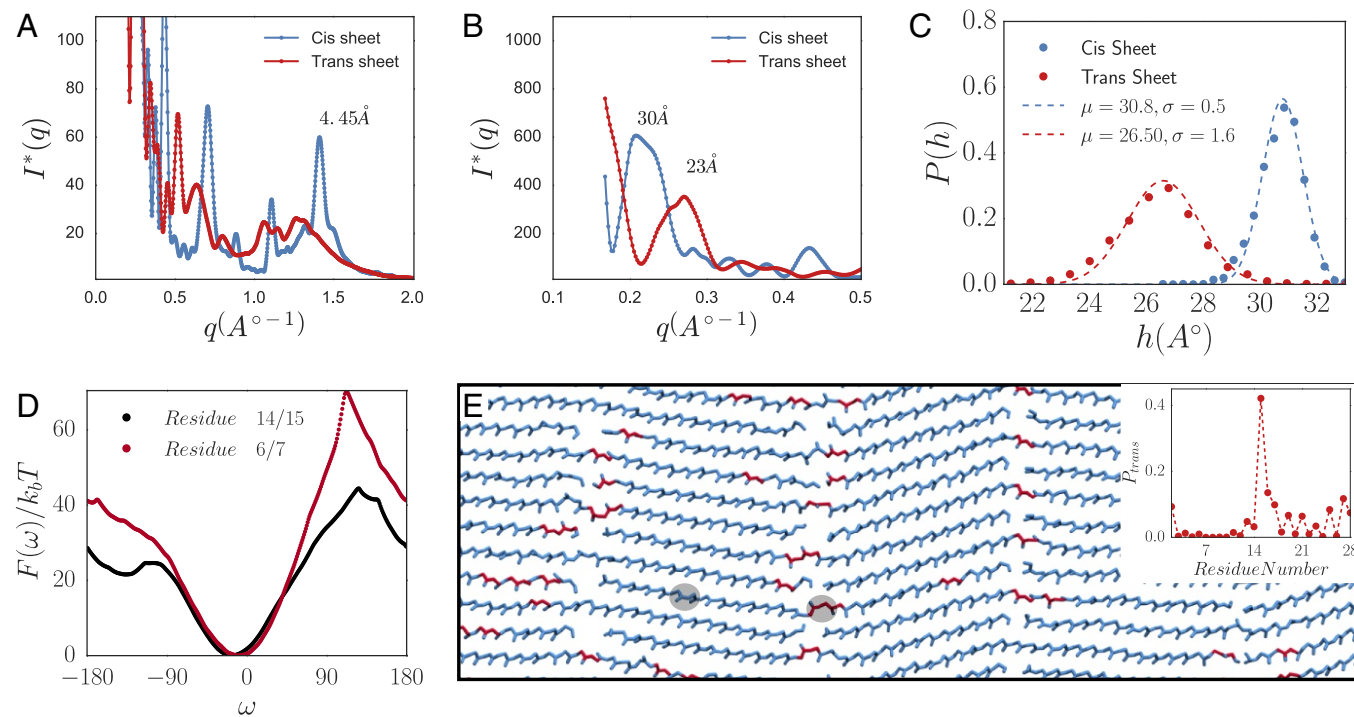AFM, atomic force microscopy; XRD, X-ray diffraction.

Fig. 3. The *cis* nanosheet's properties agree with experimental measurements. (*A* and *B*) X-ray diffraction scattering spectra [$I^*(q)$ vs. q] of the simulated *cis* and *trans* nanosheets computed using the Debye scattering equation (for details see *SI Appendix, 4. Simulation of X-ray Scattering*). (*C*) Height distribution of the simulated *cis* and *trans* nanosheets plotted together with Gaussian curves of mean μ and SD σ that best fit the data. (*D*) Free-energy profiles for rotation of the amide bond (ω) in residues 6/7 and 14/15 in a randomly chosen chain in an all-*cis* nanosheet. (*E*) Snapshot from our biased simulations (using softened dihedral angle potential terms) that reveal an increased propensity to form *trans* amides at the hinge region (residue 15) of the nanosheet. Backbone atoms are shown in blue if they are *cis* and in red if they are *trans*. The two shaded gray circles highlight residues 6/7 and 14/15 of a strand. *E*, *Inset* shows the fraction of *trans*-like residues as a function of residue number after 20 ns of our biased simulation.

show an edge-face interstrand packing pattern consistent with the molecular dynamics (MD) simulations (Fig. 2*L*).

As shown in Table 1 and Fig. 3 *A* and *B*, the dimensions of the *cis* nanosheet are in better agreement with experiment than those of the *trans* nanosheet. We note that NMR data (and indeed all experimental data summarized in this paper) are obtained from dry nanosheets. We do not have a direct probe of the charge distribution of the hydrophilic residues in the dry state. However, the consistency between the results from the dry experiments and the solvated and dry *cis*-nanosheet simulations indicates that the hydrophilic residues are likely to remain maximally charged when dried (simulation methods for dry and wet nanosheets are described in *SI Appendix, 1. Simulation setup* and *4. Simulation of X-ray Scattering*).

The models presented can be regarded as idealized all-*cis* and all-*trans* versions of the nanosheet, because no *cis–trans* isomerization events were observed during simulation [as expected from our estimates of the associated free-energy barriers (19) and experimental estimates (20)]. It is therefore not possible, using direct simulation, to sample the dihedral angle ω. NMR experiments indicate that $\approx 90\%$ of residues 7 and 8 are *cis* and $\approx 40\%$ of residue 15 are *cis*. Using enhanced sampling methods and modified potentials we found that residue 15, which sits adjacent to pockets (gaps) in the brick structure and so is less constrained than the other residues, appears to possess a propensity to adopt a near-equal mixture of *cis* and *trans*. Taking the all-*cis* model we used umbrella sampling (Fig. 3*D*) to show that the free-energy barrier for conversion of residue 15 from *cis* to *trans* is indeed less than that for residue 7. Further, an ad hoc "softening" (21) of the dihedral angle potential energy terms of the peptoid force field speeds *cis–trans* isomerization events and causes residue 15 to adopt *cis* or *trans* with roughly equal probability (Fig. 3*E*). Such features are consistent with experiment and suggest that the all-*cis* nanosheet model is a good approximation of the structure observed in experiment.

Conclusions

Our simulation results and experimental data (4) indicate that the conformations adopted by peptoids in nanosheets result from an interplay of interpeptoid contacts and the conformational preference of the backbone. Specifically, the high degree of order accessible to *cis* backbones and the resulting favorable interpeptoid interactions compensate the slight energetic strain required to maintain backbone linearity. The resulting conformation is a *cis*-Σ strand (9) in which the backbone alternates between two rotational states and remains linear and untwisted (with a kink at residue 15). Nanosheets are flat and extended—potentially useful features for sensing and catalysis—because they are built from linear and untwisted peptoid polymers. The building motif that allows peptoid linearity is their adoption of twist-opposed rotational states (9). A growing body of work shows that proteins can form similar motifs (22–25); here we have shown that experimental data and molecular modeling can inform the design of nanostructures of this type.

1. Vekilov PG, Chung S, Olafson KN (2016) Shape change in crystallization of biological macromolecules. *MRS Bull* 41:375–380.
2. Trotter J (1961) The crystal and molecular structure of biphenyl. *Acta Crystallogr* 14:1135–1140.
3. Grace CRR, et al. (2007) Structure of the N-terminal domain of a type B1 G protein-coupled receptor in complex with a peptide ligand. *Proc Natl Acad Sci USA* 104:4858–4863.
4. Hudson BC, et al. (2018) Evidence for cis amide bonds in peptoid nanosheets. *J Phys Chem Lett* 9:2574–2578.
5. Nam KT, et al. (2010) Free-floating ultrathin two-dimensional crystals from sequence-specific peptoid polymers. *Nat Mater* 9:454–460.
6. Sanii B, et al. (2011) Shaken, not stirred: Collapsing a peptoid monolayer to produce free-floating, stable nanosheets. *J Am Chem Soc* 133:20808–20815.
7. Kudirka R, et al. (2011) Folding of a single-chain, information-rich polypeptoid sequence into a highly ordered nanosheet. *Biopolymers* 96:586–595.
8. Robertson EJ, et al. (2016) Molecular engineering of the peptoid nanosheet hydrophobic core. *Langmuir* 32:11946–11957.
9. Mannige RV, et al. (2015) Peptoid nanosheets exhibit a new secondary-structure motif. *Nature* 526:415–420.
10. Pauling L, Corey RB (1951) The pleated sheet, a new layer configuration of polypeptide chains. *Proc Natl Acad Sci USA* 37:251–256.
11. Pauling L, Corey RB, Branson HR (1951) The structure of proteins: Two hydrogen-bonded helical configurations of the polypeptide chain. *Proc Natl Acad Sci USA* 37:205–211.
12. Ramachandran G, Ramakrishnan C, Sasisekharan V (1963) Stereochemistry of polypeptide chain configurations. *J Mol Biol* 7:95–99.
13. Mannige RV, Kundu J, Whitelam S (2016) The Ramachandran number: An order parameter for protein geometry. *PLoS One* 11:e0160023.
14. Heitz F, Detriche G, Vovelle F, Spach G (1981) Sheet structures in alternating poly (D, L-peptides). *Macromolecules* 14:47–50.
15. Humphrey W, Dalke A, Schulten K (1996) VMD–Visual molecular dynamics. *J Mol Graph* 14:33–38.
16. Phillips JC, et al. (2005) Scalable molecular dynamics with NAMD. *J Comput Chem* 26:1781–1802.
17. Gorske BC, Mumford EM, Conry RR (2016) Tandem incorporation of enantiomeric residues engenders discrete peptoid structures. *Org Lett* 18:2780–2783.
18. Frisch MJ, et al. (2009) *Gaussian09 Revision E.01* (Gaussian Inc, Wallingford, CT).
19. Mirijanian DT, Mannige RV, Zuckermann RN, Whitelam S (2014) Development and use of an atomistic CHARMM-based forcefield for peptoid simulation. *J Comput Chem* 35:360–370.
20. Sui Q, Borchardt D, Rabenstein DL (2007) Kinetics and equilibria of cis/trans isomerization of backbone amide bonds in peptoids. *J Am Chem Soc* 129:12042–12048.
21. Hamelberg D, Mongan J, McCammon JA (2004) Accelerated molecular dynamics: A promising and efficient simulation method for biomolecules. *J Chem Phys* 120:11919–11929.
22. Hayward S, Milner-White EJ (2008) The geometry of α-sheet: Implications for its possible function as amyloid precursor in proteins. *Proteins Struct Funct Bioinformatics* 71:415–425.
23. Hayward S, Leader DP, Al-Shubailly F, Milner-White EJ (2014) Rings and ribbons in protein structures: Characterization using helical parameters and Ramachandran plots for repeating dipeptides. *Proteins Struct Funct Bioinformatics* 82:230–239.
24. Armen RS, DeMarco ML, Alonso DO, Daggett V (2004) Pauling and Corey's α-pleated sheet structure may define the prefibrillar amyloidogenic intermediate in amyloid disease. *Proc Natl Acad Sci USA* 101:11622–11627.
25. Daggett V (2006) α-Sheet: The toxic conformer in amyloid diseases? *Acc Chem Res* 39:594–602.